SSRG International Journal of Mechanical Engineering
ISSN: 2348-8360/ https://doi.org/10.14445/23488360/IJME-V12I9P105

Volume 12 Issue 9, 46-55, September 2025

Original Article

AI based Modeling & Optimization of IRC-Enhanced Solar GT Trigeneration Systems using ANN-Evolutionary Algorithm

Mihir Kumar Pandey[1], Shrihar Pandey[2], Pankaj Kumar Shrivastava[3], Deonth Kumar[4], Manish Kumar[5], Sanjeev Kumar Sajjan[6]

[1,2]*Mechanical Engineering Department, AKS University, Satna, MP, India.*
[3,4,5,6]*Mechanical Engineering Department, Government Engineering College, Bhojpur, Ara, Bihar, India.*

[3]*Corresponding Author : psiitd@yahoo.com*

Received: 06 July 2025 Revised: 07 August 2025 Accepted: 08 September 2025 Published: 30 September 2025

Abstract *- A trigeneration system is a unified energy framework that concurrently yields three modes of energy: electricity, heating, and cooling. Solar-based Gas Turbine (GT) trigeneration systems, particularly those incorporating intercooling and reheating, are attracting significant attention due to their enhanced performance. In the present study, solar-based GT trigeneration cycle incorporating intercooling and reheating (SBIRGT) is investigated. The SBIRGT comprises a parabolic trough collector (PTC) field, pneumatic compressor, ignition chamber, gas turbine, and a single-effect LiBr absorption cooling system. Two critical productivity indicators—power output and energy efficiency—have been analyzed. Artificial Neural Networks (ANNs) were employed to develop predictive models for these outputs. To determine the optimal values for both responses, widely recognized nature-inspired optimization techniques were applied, including Rao's sequential optimization methods and Differential Evolution (DE). Among the four strategies explored, the most effective approach has been identified and recommended under the purview of this study.*

Keywords *- ANN, Optimization, DE algorithm, Rao's algorithm, Trigeneration system.*

1. Introduction

A trigeneration system concurrently yields three modes of energy, such as electricity, heat, and cooling from a one energy source, typically a gas turbine or engine. It produces electrical power, while the residual heat from the formulation process is recovered for heating applications such as space and water heating. This recovered heat is also used to operate an absorption chiller, which provides cooling for air conditioning or industrial needs. By integrating these three functions, trigeneration systems achieve greater efficiency than separate systems for power, heating, and cooling. They are widely implemented in commercial buildings, industrial facilities, and district energy networks. Key advantages include energy saving, reduced greenhouse gas emissions, and sustained cost reduction, making it a sustainable and advanced energy solution across multiple sectors [1].

The Solar-Based Gas Turbine (GT) Trigeneration Cycle (SBGTT) and the sun-driven interstate cooling and Reheated GT Trigeneration (SBIRGT) cycle are thermodynamic systems that utilize solar energy to simultaneously generate electricity, heating, and cooling. The basic GT trigeneration cycle uses a simple gas turbine powered by solar thermal energy, with waste heat used for heating and cooling. It is simpler and cost-effective, but offers lower efficiency.

The intercooled and reheated GT trigeneration cycle improves efficiency by incorporating intercooling (between compression stages) and reheating (between numerous stages), by using numerous solar heat inputs. This configuration is more complex, but provides higher thermal efficiency and better performance. The main difference lies in the advanced thermodynamic enhancements of the latter, which lead to improved energy utilization.

Author previously presented a thermal performance analysis of a solar-dependent interstate cooling and reheating Gas Turbine (GT) trigeneration system using a trough solar concentrator and MATLAB 2018. The study was conducted in three phases: validation of the SBGTT, investigations and optimization of an SBGTT and comparison of an SBIRGT. Results show increasing power output and efficiency across the stages, with the final configuration producing 41.0 MW power at 0.527 kg/s NG flow, and achieving thermodynamic

performances in terms of energy and exergy of 39.7 % and 40.9 %. This study claims uniqueness and novelty in its approach.

Singh et al. [2] explored a heliostat-driven CSP system using a triple combined cycle that integrates three different thermodynamic cycles. It investigated performance improvements through interstate cooling and heating in the GT cycle, with exhaust heat recovery via two different arrangements: a waste heat vapor generator (HRVG) and a waste heat steam generator (HRSG). Thermodynamic analysis (using the first and second laws) showed that the HRVG setup achieves a highest energy performance of 63.54% and exergetic performance of 38.37%, while the HRSG setup performs slightly better, reaching 64.15% and 39.72%, respectively. Dabwan et al. [3] introduced an innovative hybrid SBIRGT system using a linear Fresnel solar field to pre-combustion air heating before combustion. Compared to the conventional Solar Preheating GT (SPGT), the SBIRGT showed significantly better performance, with a 19.5% increase in fuel-based efficiency (vs. 0.26% for SPGT) and reduced SFC (7017 kJ/kWh vs. 10358 kJ/kWh). It was also more economical, achieving a lower levelized electricity cost (4.34 US¢/kWh vs. 5.15 US¢/kWh). Additionally, it reduces fuel use and CO_2 emissions by about 19.3%. Abubaker et al. [4] addressed numerous important challenges of GT power plants—high fuel consumption, heat loss, and sensitivity to ambient temperature—by integrating sun-driven preheating and cooling systems. Using parabolic trough collectors, air was preheated before combustion and cooled before compression via an absorption cooling cycle.

The proposed system improves power output by 6.87%, reduces fuel consumption by 10.53%, and increases thermal efficiency by 19.45%. It also lowers combustion emissions. Web diagrams were used to analyze the influence of system condition on performance and environmental impact. Rovira et al. [5] explored unified solar hybrid cycles employing GT with fractional recuperation and solar integration at varying pressure states. The study compared different configurations to enhance solar-to-electricity conversion efficiency. Javaherian et al. [6] explored a biomass-based cogeneration system combining a GT with a Rankine and a gas absorption cycle, evaluated from thermal performance perspectives. Biomass gasification (using wood) provided fuel for the gas turbine, while solar energy preheats the Rankine cycle fluid to enhance efficiency. Waste heat is recovered via an absorption cooling cycle. A multi-objective optimization targeted maximum thermal performance and minimum CO_2 emissions. The gasification reactor and combustor were the main sources of thermal performance destruction (46.7% and 22.9%). Parametric analysis showed optimal performance at a Pressure Ratio (PR) of 10, and a 1% drop in compression ratio could be offset by a 9.30 % enhancement in solar contribution. Munoz et al. [7] reviewed the main components of solar heat-based power plants, specifically the solar array and energy block and emphasized how the choice of thermodynamic cycle and working fluid impacts performance. While the steam Rankine cycle, commonly paired with parabolic trough collectors, is the most widely used, other configurations like integrated solar combined cycles are also implemented. The study discussed conventional cycles, their benefits, and challenges, particularly in hybrid solar-fossil fuel systems. It also analyzed advanced configurations that offer performance advantages under specific conditions. Lastly, it briefly examined the integration/hybridization of solar thermal with alternative energy sources.

Rovira et al. [8] demonstrated a modern integrated solar power cycle configuration featuring a reclaiming GT and a recently developed Dual Reclaiming Double Expansion (DRDE) cycle using propane. Replacing the conventional Rankine cycle, this setup reduced fuel consumption while maintaining sufficient exhaust temperatures for the DRDE cycle. Solar energy was supplied by a solar trough collector with liquid as the energy-transferring medium, and optimal solar integration is analyzed. Performance assessments at two locations showed that the proposed ISCC-R-DRDE system achieves lower heat rates and a reduced Levelized Cost Of Energy (LCOE) compared to conventional ISCC systems, highlighting its potential as an efficient future technology. Khan et al. [9] analyzed an interstate cooled reheat gas/steam mixed cycle integrated with CO_2 retention and methanation. Captured CO_2 was converted into methane for reuse as fuel, reducing emissions. An ORC system was added between compressors to utilize intercooling heat, with working fluids selected based on favorable thermophysical properties. Thermodynamic and parametric analyses showed that lower cycle pressure ratios enhance steam generation and work output. The integration of the carbon capture unit increases overall system performance from 220.90 MW to 370.00 MW at a Turbine Input Temperature (TIT) of 1480.0 K, demonstrating significant performance gains. Shukla et al. [10] presented a thermal performance evaluation of a sun energy-driven three-stage hybrid GT cycle designed to give zero-emission electricity. The system included a Brayton cycle with intercooling as the topping cycle, and a steam Rankine and ORC system as bottoming cycles. Heat rejected during intercooling is utilized in the ORC, while turbine exhaust energy is used in the SRC. The performance was analyzed using three different ORC fluids, with R245fa yielding the best results—achieving a peak performance efficiency of 21.89% and a power output of 218.98 kJ/kg air at a PR of 31. Dupuy et al. [11] reviewed the current state of trigeneration (CCHP) systems as a sustainable alternative to fossil fuels for meeting rising energy demands, particularly in cooling applications. They presented their applications, performance indicators, comparisons with conventional systems, and reported improvements and emerging concepts. The review also emphasized renewable energy-based low-temperature CCHP technologies, serving as a foundation for future exergo-economic optimization studies.

The existing research on SBIRGT indicates that the process still requires significant development, especially in light of the current advancements in artificial intelligence. In this study, two key performance metrics—efficiency and power output—have been examined using PR, TIT, and air Mass Flow Rate (MFR) as design parameters. Artificial Neural Network (ANN) models were employed for both efficiency and power output, with Mean Squared Error (MSE) used as the performance criterion. These ANN models were then employed as objective functions to identify optimal solutions for both outputs using Rao's sequential optimization techniques and the Differential Evolution (DE) method. Among the four resulting solutions, the most effective one has been recommended within the scope of this research.

2. Method

2.1. Artificial Neural Network

An ANN is a relatively recent mathematical modeling tool, particularly useful for predicting Multifaceted, unpredictable, and complex process patterns. Similar to the Mental faculties, it consists of a matrix of interconnected neurons that work together to route data efficiently. The popular back-propagation ANN algorithm (FFBANN) is an easy and well-accepted ANN model. In a fully linked FFBANN, each neuron in a given layer gets signals from all the neurons in the antecedent layer. The commonly used composition of this ANN algorithm is shown in Figure 1.

A typical network is made up of multiple layers, each embedding neurons, which are categorized as the input, intermediate, and prediction layers. Connection weights and offset parameters are essential components of a network as well. The primary signal, based on the control parameters, is fed into the first layer (the input layer) and processed by an appropriate Transfer Function (TF). The counteraction associated with each neuron is then passed to the next layer, and this process continues until a specified criterion is met. Each neuron typically consists of a weight, bias, and an activation function. The neuron's inputs are initially aggregated, as shown in Equation (1) [12, 13]:

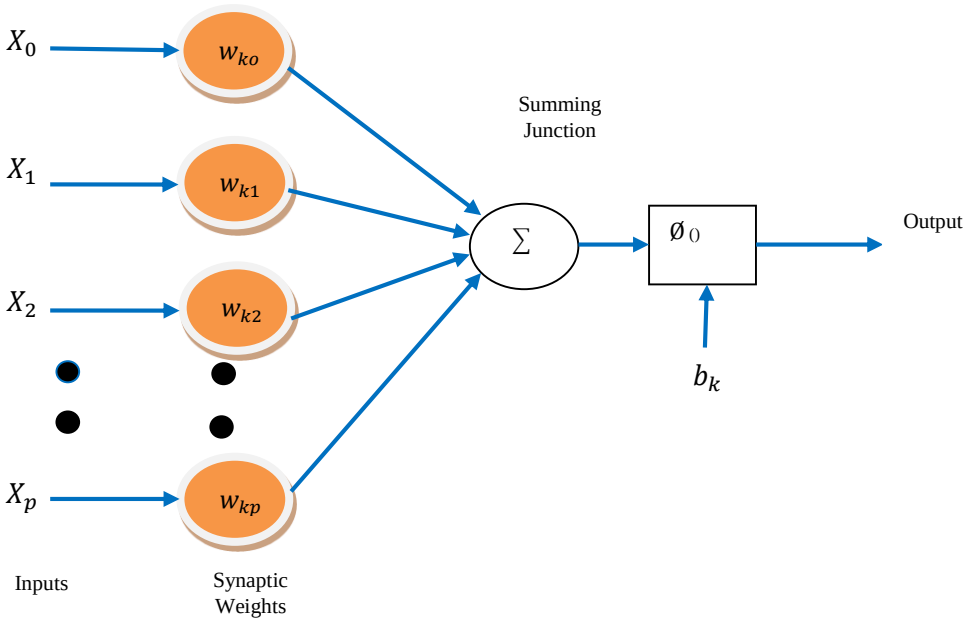

Fig. 1 ANN mathematical model structure

$$net_r = \sum_{i=1}^{N} w_{kr} X_k + b_r \quad (1)$$

Here, w_{kr} depicts the connection weights supplied to rth neuron in a defined layer from the prior stage, and b_r is the offset parameter. The response developed by a suitable apt TF during the aggregation of the supply required target Y_r from the neuron as mentioned below:

$$Y_r = F(net_r) \quad (2)$$

2.2. RAOs Method

Rao's Optimization Method is a simple, parameter-free metaheuristic algorithm based on mathematical principles rather than natural processes. It maintains a collection of trial solutions and randomization to explore the solution space. The method is easy to implement, requires no tuning, and is effective for continuous, nonlinear, and multimodal optimization problems. It is applied in fields like engineering design, power systems, and machine learning optimization. In the present study, Artificial Neural Network (ANN) models were initially developed to predict efficiency and power output. These models were then maximized by adopting Rao's sequential optimization approaches and the Differential Evolution (DE) algorithm [14, 15]. The implementation of these techniques to solve the defined Objective Functions (OF) is detailed below:

Roa-1: $U_i^{(k)} = U_i^{(k-1)} + r[U_{best}^{(k-1)} - U_{worst}^{(k-1)}]$ (3)

or

Roa-2: $U_i^{(k)} = U_i^{(k-1)} + r_1\left[U_{best}^{(k-1)} - U_{worst}^{(k-1)}\right] + r_2\left[\left|U_i^{(k-1)} \; or \; U_l^{(k-1)}\right| - \left|U_l^{(k-1)} \; or \; U_i^{(k-1)}\right|\right]$ (4)

or

Roa-3: $U_i^{(k)} = U_i^{(k-1)} + r_1\left[U_{best}^{(k-1)} - \left|U_{worst}^{(k-1)}\right|\right] + r_2\left[\left|U_i^{(k-1)} \; or \; U_l^{(k-1)}\right| - \left|U_l^{(k-1)} \; or \; U_i^{(k-1)}\right|\right]$ (5)

The three algorithms above vary depending on the vector $U_i^{(k)}$

r, r_1 and r_2 denoted a random value within the range of 0 to 1.

$U_i^{(k-1)} \; or \; U_l^{(k-1)}$ allude

$= U_i^{(k-1)}$, if $U_i^{(k-1)}$ is an upgraded result vector in comparison with $U_l^{(k-1)}$

$= U_l^{(k-1)}$, else

$U_l^{(k-1)} \; or \; U_i^{(k-1)}$ implies

$= U_l^{(k-1)}$, if $U_l^{(k-1)}$ is an upgraded result vector in comparison with $U_i^{(k-1)}$

$= U_i^{(k-1)}$, else

The equations above are suggested to refresh current results using the above-discussed algorithms.

Step-1: Create the population of dimension 'm', in the range of $\left[U_{ij}^{min} \le U_{ij} \le U_{ij}^{max}\right]$ $\left[U_{ij}^{min} \le U_{ij} \le U_{ij}^{max}\right]$, j = 1,2,3, … . , D $U_i^{(0)} = \left[u_{1i}^{(0)}, u_{2i}^{(0)}, \ldots\ldots\ldots\ldots, u_{ki}^{(0)}\right]^T$,

Step-2: Run the program for each U_i^m .

Step-3: Is the population set viable? if yes, then go to step-4, or else enhance the bus quantity $k = k + 1$, and repeat to step-1.

Step-4: Get $U_{best}^{(0)}$ and $U_{worst}^{(0)}$ depending upon the desirable (OF) (J). i.e. $J\ (U_i^{(0)})$.

Step-5: Fix trek number, $k = 1$.

Step-5: Get improved solutions using relations (1), (2) and (3), respectively and individually for all three Rao's algorithms. i.e. $U_i^{(k)}$, $i = 1,2,3, \ldots\ldots\ldots, m$

Step-6: For every improved solution $U_i^{(k)}$, check the value of OF, i.e. Effi ($U_i^{(k)}$) and Power ($U_i^{(k)}$) by executing the program.

Step-7: Categorize every improved candidate solution $U_i^{(k)}$ as viable (F) or Not viable (NF), depending upon the results in step-6. i.e.

$U_i^{(k)}$ - is 'F' if all boundaries are under the threshold.

$U_i^{(k)}$ - is 'NF' if any of the constraints are transgressed beyond the limit.

Step-8: Modify the population in the following way:

$U_i^{(k)} = U_{i,}^{(k-1)}$, $if \;\; U_i^{(k)} \; is \; NF$

$= U_{i,}^{(k)}$, $if \;\; U_i^{(k)} \; is \; 'F'$ and $J(U_i^{(k)}) < J(U_i^{(k-1)})$

Step-9: Hence, the step-8 promise in the modified population, all vectors are 'F'.

Obtain $U_{best}^{(k)}$ and $U_{worst}^{(k)}$.

Step10: Increment the iteration count $k = k + 1$, if $k > k_{max}$,

Stop.

Else, start again using step number 5.

3. Experimental Details

The layout of the SBICRGT trigeneration system discussed in this study is given below in Figure 2.

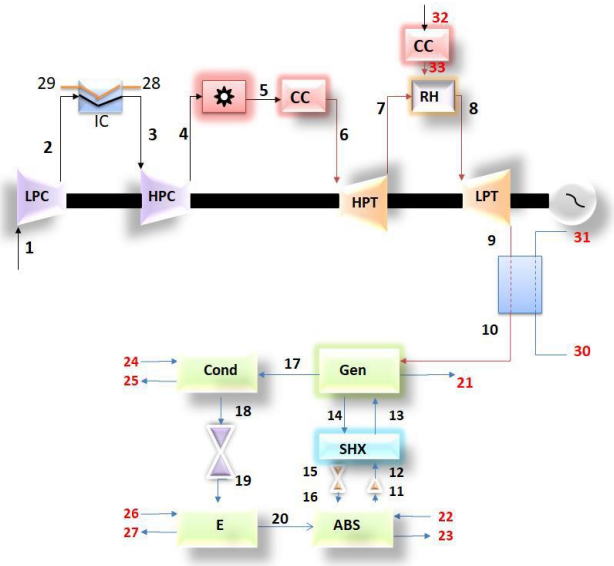

Fig. 2 Schematic of SBIRGT trigeneration system [16]

The system comprises a Parabolic Trough Collector (PTC) field, Low and High Pressure Compressors (LPC/HPC), Intermediate Cooler (IC), ignition chamber (CC), High and Low Pressure Turbines (HPT/ LPT), reheat exchanger (RH), and a single-effect LiBr absorption refrigeration cycle (ARC). Ambient air enters the LPC and is pressurized from state 1 to stage 2. It then passes through the interstate cooler, where it releases heat to the environment,

exiting at state 3 before entering the HPC. The air is further compressed to state 4 and routed through the solar collector field. At state 5, the air gains heat at a constant pressure and then flows into the Combustion Chamber (CC). In the CC, fuel is added, increasing the temperature and pressure of the air to state 6.

The high-energy gas expands through the HPT from state 6 to state 7 and is subsequently reheated in the RH to reach state 8. It then enters the LPT, where it expands further from state 8.0 to 9.0, producing effective mechanical work that is transformed to electricity via a generator. The exhaust gases at state 9 are directed to a heat recovery unit, which provides thermal energy to drive the single-effect LiBr ARC for cooling applications.

The input data for SBICRGT were obtained from Bellos and Tzivanidis [16] and Anvari et al. [17]. The PR, TIT, and MFR of air, as listed in Table 1, were used as input control factors, while energy efficiency and power output served as target control factors. The design matrix for the input and target control factors is presented in the Tables below.

Table 1. Description of input variables

Parameters	Pressure Ratio (X_1)	TIT (X_2)	MFR(X_3)
Low (1)	4	800	10
Central (2)	6	1000	20
High (3)	8	1200	30

Table 2. Data for SBIRGT

Exp. No	Pressure Ratio (X_1)	TIT (X_2)	MFR (X_3)	Efficiency	Power Output (KW)
1	2	2	2	43.5	170.5
2	1	1	2	38.5	132.44
3	2	2	2	43.5	170.5
4	1	3	2	43	169.15
5	2	3	1	42.5	93.5
6	2	3	3	46.0	280.5
7	3	3	2	48.0	211.2
8	3	1	2	44.0	176.0
9	3	2	1	44.0	96.8
10	2	2	2	43.5	170.8
11	1	2	3	43	226.05
12	2	1	1	39.5	77.2
13	1	2	1	40.0	75.25
14	3	2	3	48.0	290.4
15	2	1	3	42.5	231.66

4. Parametric Exploration, Model Development and Optimization (PEMDO)

4.1. PEMDO for Efficiency

4.1.1. Parametric Explorations for Efficiency

The test frequently used for comparing group means, identified as variance analysis (ANOVA) [18], to assess the influential input parameters is portrayed in Table 3.

Table 3. Efficiency evaluation through ANOVA

Component	DOF	Adj SS	Adj MS	F	Impact (%)
Pressure Ratio	2	122.6	122.6	1142.52	48.80
TIT	2	77.45	77.45	721.55	28.52
Mass Flow Rate	2	61.42	61.42	572.02	22.48
Error	8	1.825	2.0		
Total	14	263.5			

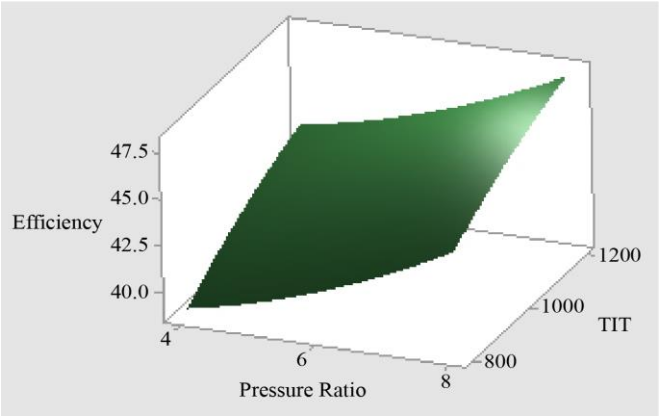

Fig. 3 Pressure ratio versus TIT for efficiency during SBIRGT

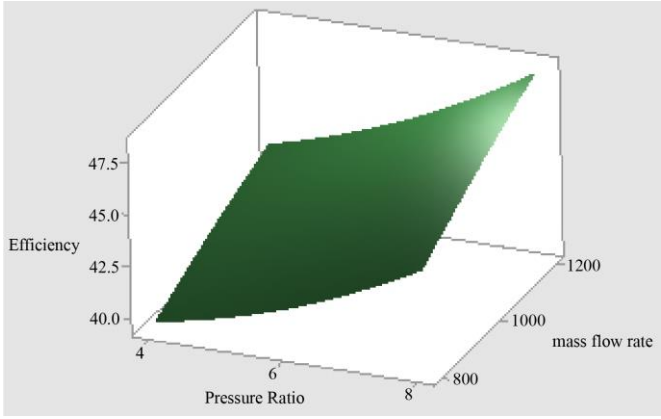

Fig. 4 Pressure ratio versus MFR for efficiency during SBIRGT

Containing the F-statistics of 1142.5, the pressure ratio is recognized as the primary contributing factor (with a contribution of 48.80%) variable during SBICRGT for efficiency. With an F-value of 721.55, the TIT turns out to be the second most influential variable (with a contribution of 28.22%), followed by MFR. Figure 3 presents a three-dimensional plot illustrating the variation of efficiency with PR and TIT.

The graph clearly shows that as the PR increases from 4 to 8, the efficiency exhibits a consistent upward trend, rising from 39% to 48%. Similarly, analyzing the influence of TIT, it is evident that higher TIT values positively impact efficiency. As TIT climbs from 800 K to 1200 K, the efficiency improves significantly. Figure 4 displays a three-dimensional plot of efficiency versus PR and MFR. Consistent with the trends observed for other parameters, efficiency also increases with rising MFR, indicating a strong positive correlation.

4.1.2. Model Development for Efficiency

To develop the efficiency model of SBICRGT using Artificial Neural Networks (ANN), MATLAB R2023b software was employed. The software offers three activation (transfer) functions: pure linear, sigmoid (logistic), and tanh (hyperbolic tangent). Various combinations of these activation functions were tested in both the hidden (intermediate) and output layers to determine the configuration that yielded the lowest Mean Squared Error (MSE). After extensive experimentation, the following MSE values were observed:

- Linear–Linear combination (intermediate and output layers): 0.0906
- Sigmoid–Linear combination: 5.99×10^{-5}
- Tanh–Linear combination: 1.25×10^{-10}

The results clearly indicate that using the tanh activation function in the intermediate layer and a linear function in the output layer produces the lowest MSE, making it the most suitable configuration for modeling efficiency.

Additionally, it was found that the optimal ANN architecture for efficiency includes three neurons in the hidden layer. The final ANN model was constructed using the identified transfer functions, along with the corresponding weights and biases, and is presented in mathematical form below.

$$Efficiency = 0.5281 * y_1 + 0.866 * y_2 + 0.946 * y_3 + 0.899 \quad (8)$$

Where,

$$y_1 = \tanh(4.536 * x_1 + 0.9881 * x_2 + 0.8693 * x_3 - 2.0559)$$

$$y_2 = \tanh(4.5554 * x_1 - 0.7853 * x_2 + 0.6542 * x_3 + 3.4141)$$

$$y_3 = \tanh(-0.9574 * x_1 - 0.6556 * x_2 - 0.4573 * x_3 - 0.9766)$$

4.1.3. Maximization of Efficiency

Each of the four optimization algorithms was applied to the developed ANN-based efficiency model. The optimization routines were implemented using MATLAB R2023b. The efficiency maximization problem involved three key decision variables-x_1, x_2, and x_3-with the following bounds:

$4 \le x_1 \le 8,$
$800 \le x_2 \le 1200,$
$10 \le x_3 \le 30.$

To begin the optimization process, 50 initial candidate solutions for each variable were randomly generated in Excel, considering the specific distribution characteristics of each parameter. Although the iteration bound was set to 1000, the optimization was concluded after 800 iterations due to efficiency improvement stagnation.

Table 4 presents a comparative summary of the best solutions obtained by the four algorithms as discussed.

Table 4. Comparison of different algorithms for optimization of efficiency during SBIRGT

Methodology	U_1	U_2	U_3	Efficiency	No. of iterations
Rao-3	7.99	1198.99	30.00	50.6%	500
Rao-2	8.00	1198.99	29.394	49.33%	625
Rao-1	8.00	1199.98	29.554	46.69%,	650
DE	7.879	1197.97	29.444	47.38%	550

Table 5 offers a detailed statistical comparison based on various statistical parameters as shown in the Table.

Figure 5 illustrates the relationship between efficiency and generation count, based on the best-performing design variables from the Rao and DE algorithms.

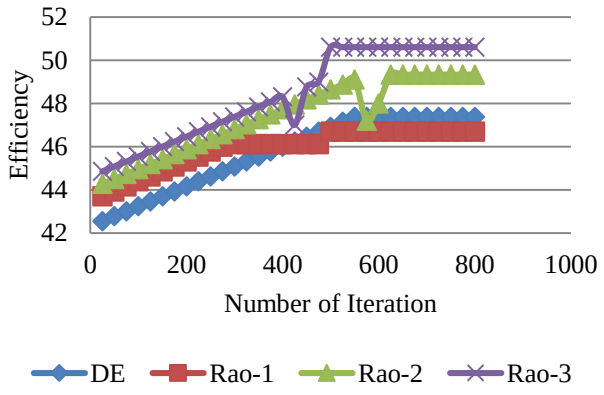

Fig. 5 Iteration-based convergence plot for efficiency maximization during SBIRGT

Table 5. Statistical evaluation of efficiency

Optimization techniques	Arithmetic mean value of the Efficiency	Median value of the Efficiency	Mean Deviation of Efficiency	Variance of Efficiency	Standard deviation of Efficiency	Best value of Efficiency	Worst value of Efficiency	Frequency of convergence	Confidence level	Determined value for the Engg.	Standard error of the mean Efficiency	Confidence interval of the Efficiency	Length of confidence interval of the Efficiency
	$\overline{\text{Efficiency}}$	m	d	s	σ	$\text{Effi}_{\text{BEST}}$	$\text{Effi}_{\text{WorstEST}}$	f	γ	c	ε	μ	L
Rao-3	53.761	53.677	3.70E-06	0.25E-03	0.0536	53.8924	53.8484	13	0.95	2.0452	0.0068	$53.761 \leq \mu \leq 53.677$	0.0338
Rao-2	52.820	52.914	3.25E-06	0.25E-03	0.0358	42.861	14	13	0.95	2.0452	0.0082	$52.820 \leq \mu \leq 2.8208$	0.0385
Rao-1	52.777	52.870	0.45E-06	0.86E-03	0.0477	42.836	42.756	10	0.95	2.0452	0.0246	$52.777 \leq \mu \leq 2.7945$	0.0526
DE	52.697	52.789	52.0E-06	4.87E-03	0.052	42.774	42.644	10	0.95	3.0552	0.0168	$52.697 \leq \mu \leq 2.6976$	0.0698

The optimized efficiency values obtained using DE, Rao-1, Rao-2, and Rao-3 methods were 47.38%, 46.69%, 49.33%, and 50.6%, respectively. These performances clearly demonstrate that the Rao-3 optimization strategy outperformed the others, delivering the highest global optimum efficiency.

4.2. PEMDO for Power

4.2.1. Parametric Explorations for Power

ANOVA, a commonly used test for comparing group means, was leveraged to evaluate the impact of input parameters, with the results summarized in Table 6.

Table 6. Power output evaluation through ANOVA

Component	DOF	Adj SS	Adj MS	F	Impact (%)
Pressure Ratio	2	8282	8282	8282	5.55
TIT	2	5437	5437	6661	3.84
Mass Flow Rate	2	132585	132585	162435	90.92
Error	8	13	0.000007		
Total	14	133018			

The Mass Flow Rate (MFR) emerged as the most significant factor affecting power output in SBICRGT, with an F-value of 162435 and a contribution of 90.92%. The Pressure Ratio (PR) was identified as the second most influential parameter, with an F-value of 10146 and a contribution of 5.55%, followed by the Turbine Inlet Temperature (TIT). Figure 6 presents a three-dimensional plot illustrating power output as a function of PR and MFR. The graph clearly shows that as MFR increases from 10 to 30, power output consistently rises from 75 kW to 290 kW. In contrast, Figure 7 indicates that power output remains relatively constant with changes in PR.

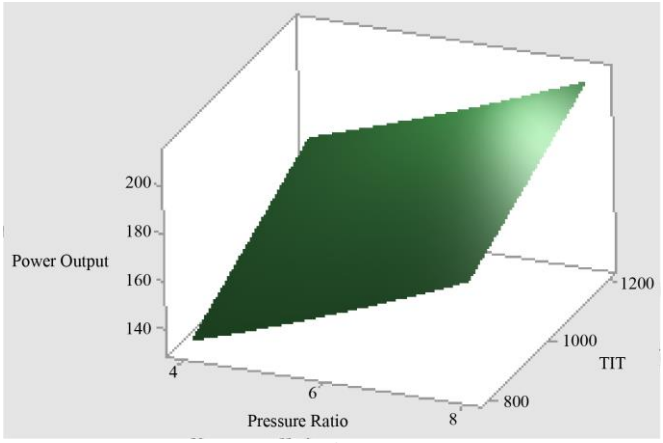

Fig. 6 Pressure ratio versus TIT for power output during SBIRGT

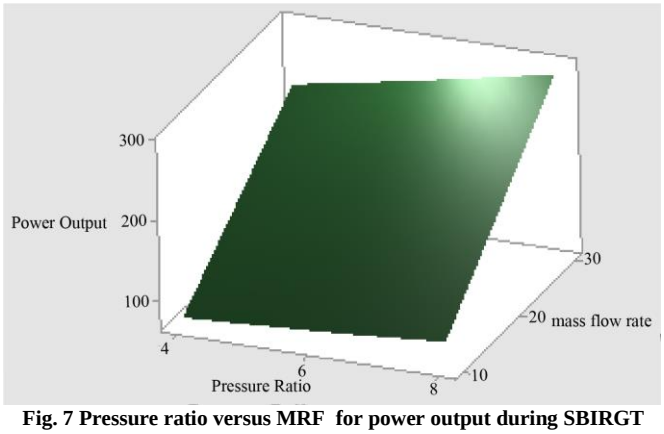

Fig. 7 Pressure ratio versus MRF for power output during SBIRGT

4.2.2. Model Development for Power

For power output prediction, the Mean Squared Error (MSE) was evaluated for different combinations of Transfer

Functions (TFs). The combination of linear TF in both the intermediate and output layers resulted in an MSE of 0.0899. Using the Sigmoid (Logistic) TF in the intermediate level and linear TF in the output level yielded an improved MSE of 1.9 × 10^{-7}. However, the lowest MSE of 5.55 × 10^{-12} was achieved with the Tanh (Hyperbolic Tangent) TF in the intermediate layer and linear TF in the output layer.

Similar to the findings for efficiency modeling, the Tanh–linear combination proved to be the most effective for modeling power output as well. Therefore, this configuration was adopted for the power output model. The corresponding mathematical representation of the power output using the AI-based model—incorporating the selected transfer functions, connection weights, and bias terms—is presented below:

$$Power = 120.029 * y_1 - 5.65 * y_2 + 0.6990 * y_3 + 0.7645 \quad (9)$$

Where,

$$y_1 = \tanh(0.2250 * x_1 + 4.062 * x_2 + 0.4462 * x_3 - 5.503)$$

$$y_2 = \tanh(-2.455 * x_1 + 4.555 * x_2 + 0.6435 * x_3 + 0.0665)$$

$$y_3 = \tanh(-0.3345 * x_1 - 0.4548 * x_2 - 0.5433 * x_3 + 3.0555)$$

4.2.3. Maximization of Power

Each of the four optimization algorithms was applied to the developed ANN model for power output. The software implementation for each algorithm was carried out using MATLAB R2023b. The power maximization problem involved three key input parameters:

$4 \le x_1 \le 8,$
$800 \le x_2 \le 1200,$
$10 \le x_3 \le 30.$

Initially, 50 individuals for each variable were randomly generated in Excel, based on the statistical distribution of each parameter. Although the iterations bound was set at 900, the optimization process was aborted after 600 iterations due to stagnation in the power output.

Table 7. Comparison of different algorithms for optimization of power output during SBIRGT

Methodology	U_1	U_2	U_3	Power	No. of iterations
Rao-3	**8.00**	**1199.05**	**30.00**	**331.2**	**600**
Rao-2	7.95	1199.95	29.99	305.2	675
Rao-1	7.889	1200.00	29.554	267.95	525
DE	7.879	1197.97	29.444	269.1	575

Table 7 presents a comparative summary of the best solutions obtained by the four algorithms as discussed. Table 8 provides a detailed comparison of the algorithms using statistical metrics.

Figure 8 shows the variation of power output with iteration count for the best-performing parameters identified by the Rao and DE algorithms.

Table 8. Statistical evaluation of power output in Rao's metaphor-less and DE algorithms

Optimization techniques	Arithmetic mean value of the power	Median value of the T power	Mean deviation of power	Variance of T power	Standard deviation of power	Best value of power	Worst value of power	Frequency of convergence	Confidence level	Determined value for the Engg. Application	Standard error of the mean power	Confidence interval of the power	Length of the confidence interval of the power
	$\overline{\mathbf{power}}$	m	d	s	σ	$\mathbf{power}_{BES}$	$\mathbf{power}_{Wo}$	f	γ	c	ε	μ	L
Rao-3	**380.16**	**380.16**	**0.36E-05**	**0.083E-06**	**0.29E-03**	**0.037**	**0.0465**	**14**	**0.95**	**4.0652**	**0.22E-03**	**$0.01432 \le \mu \le 0.01430$**	**0.57E-03**
Rao-2	378.14	378.14	0.35E-05	0.362E-06	0.54E-03	0.037	0.0467	11	0.95	4.0652	0.29E-03	$0.01679 \le \mu \le 0.01647$	0.87E-03
Rao-1	376.15	376.15	0.33E-05	0.55E-06	0.78E-03	0.0458	0.0297	13	0.95	4.0452	0.39E-03	$0.01810 \le \mu \le 0.02871$	1.87E-03
DE	375.20	375.20	0.30E-05	0.887E-06	0.80E-03	0.0567	0.0440	10	0.95	4.0462	0.43E-03	$0.01985 \le \mu \le 0.01915$	2.44E-03

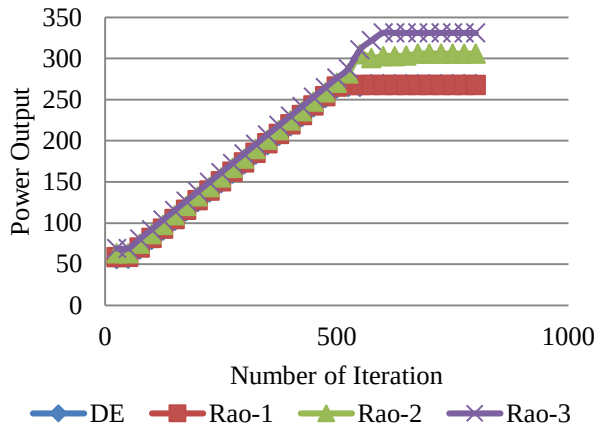

Fig. 8 Iteration-based plot for power maximization during SBIRGT

The optimized power values achieved using DE, Rao-1, Rao-2, and Rao-3 were 269.1 kW, 267.95 kW, 305.2 kW, and 331.2 kW, respectively. This clearly indicates that the Rao-3 algorithm outperforms the others by delivering the most optimal global result. ANNs can capture complex nonlinear relationships between input and output variables that conventional linear/statistical models struggle with. Also, ANNs can process multiple input parameters simultaneously without simplifying assumptions. Unlike conventional optimization methods, which may get stuck in local minima, evolutionary algorithms explore the entire search space and hence give better results.

5. Conclusion

The modeling and optimization of SBIRGT systems have been carried out using Artificial Neural Networks (ANN), Rao's sequential optimization methods, and differential evolution. The key observations from current work are summarized as follows:

1. The pressure ratio was identified as the most influential input control factor affecting efficiency in the SBIRGT system, while the mass flow rate of air had the greatest impact on power output.
2. The turbine inlet temperature was found to be the second most significant factor influencing both efficiency and power output in the SBIRGT system.
3. Using Mean Squared Error (MSE) as the evaluation metric, the ANN models for both efficiency and power output demonstrated high accuracy, with minimal MSE values for each.
4. Among the four evolutionary optimization algorithms evaluated, Rao-3 exhibited the highest performance in this study.
5. The integrated approach combining ANN with Rao-3 resulted in significant enhancements, achieving a 5.55% increase in efficiency and a 13.75% improvement in power output.

Funding Statement

This research was carried out without financial support from governmental, commercial, or charitable funding bodies.

References

[1] K.J. Chua et al., "Integrating Renewable Energy Technologies to Support Building Trigeneration – A Multi-Criteria Analysis," *Renewable Energy*, vol. 41, pp. 358-367, 2012. [CrossRef] [Google Scholar] [Publisher Link]

[2] Onkar Singh, Gaitry Arora, and Vinod Kumar Sharma, "Energy-Exergy Analysis of Solarized Triple Combined Cycle Having Intercooling, Reheating and Waste Heat Utilization," *Tecnica Italiana-Italian Journal of Engineering Science*, vol. 65, no. 1, pp. 93-104, 2021. [CrossRef] [Google Scholar] [Publisher Link]

[3] Yousef N. Dabwan et al., "A Novel Hybrid Solar Preheating Intercooled Gas Turbine Based on Linear Fresnel Reflector," *Journal of University of Science and Technology of China*, vol. 51, no. 7, pp. 505-520, 2021. [CrossRef] [Google Scholar] [Publisher Link]

[4] Ahmad M. Abubaker et al., "Energy and Environmental Analyses of a Solar–Gas Turbine Combined Cycle with Inlet Air Cooling," *Sustainability*, vol. 16, no. 14, pp. 1-31, 2024. [CrossRef] [Google Scholar] [Publisher Link]

[5] Antonio Rovira et al., "Integrated Solar Combined Cycles Using Gas Turbines with Partial Recuperation and Solar Integration at Different Pressure Levels," *SOLARPACES 2016: International Conference on Concentrating Solar Power and Chemical Energy Systems: AIP Conference Proceedings*, Abu Dhabi, United Arab Emirates, vol. 1850, no. 1, pp. 1-10, 2017. [CrossRef] [Google Scholar] [Publisher Link]

[6] Amirreza Javaherian et al., "Two-Objective Optimization of a Cogeneration System Based on a Gas Turbine Integrated with Solar-Assisted Rankine and Absorption Refrigeration Cycles," *Sustainability*, vol. 15, no. 21, pp. 1-27, 2023. [CrossRef] [Google Scholar] [Publisher Link]

[7] Marta Muñoz, Antonio Rovira, and María José Montes, "Thermodynamic Cycles for Solar Thermal Power Plants: A Review," *WIREs Energy and Environment*, vol. 11, no. 2, pp. 1-19, 2022. [CrossRef] [Google Scholar] [Publisher Link]

[8] Antonio Rovira et al., "Analysis of an Integrated Solar Combined Cycle with Recuperative Gas Turbine and Double Recuperative and Double Expansion Propane Cycle," *Entropy*, vol. 22, no. 4, pp. 1-20, 2020. [CrossRef] [Google Scholar] [Publisher Link]

[9] Razzak Khan et al., "Thermodynamic Investigation of Intercooled Reheat Gas Turbine Combined Cycle with Carbon Capture and Methanation," *Materialstoday Proceedings*, vol. 38, no. 1, pp. 449-455, 2021. [CrossRef] [Google Scholar] [Publisher Link]

[10] Anoop Kumar Shukla et al., "Thermodynamic Investigation of Solar Energy-Based Triple Combined Power Cycle," *Energy Sources, Part A: Recovery, Utilization, and Environmental Effects*, vol. 41, no. 10, pp. 1161-1179, 2019. [CrossRef] [Google Scholar] [Publisher Link]

[11] Arthur Dupuy et al., "Trigeneration Systems: A State-of-the-Art Review," *Energies*, vol. 18, no. 10, pp. 1-32, 2025. [CrossRef] [Google Scholar] [Publisher Link]

[12] Mahendra Raj Singh, Pankaj Kumar Shrivastava, and Pushpendra Singh, "Optimization of EDM Process of Titanium Alloy using EPSDE Technique," *Multiscale and Multidisciplinary Modeling, Experiments and Design*, vol. 4, pp. 121-130, 2021. [CrossRef] [Google Scholar] [Publisher Link]

[13] Pankaj Kumar Shrivastava, and Avanish Kumar Dubey, "Intelligent Modeling and Multiobjective Optimization of Electric Discharge Diamond Grinding," *Materials and Manufacturing Processes*, vol. 28, no. 9, pp. 1036-1041, 2013. [Google Scholar] [Publisher Link]

[14] L.D. Arya, Pushpendra Singh, and L.S. Titare, "Optimum Load Shedding Based on Sensitivity to Enhance Static Voltage Stability Using DE," *Swarm and Evolutionary Computation*, vol. 6, pp. 25-38, 2012. [CrossRef] [Google Scholar] [Publisher Link]

[15] Pushpendra Singh et al., "Optimum Value based under Voltage Load Shedding Strategies," *Australian Journal of Electrical and Electronics Engineering*, vol. 18, no. 3, pp. 146-160, 2021. [CrossRef] [Google Scholar] [Publisher Link]

[16] Evangelos Bellos, and Christos Tzivanidis, **"**Optimization of a Solar-Driven Trigeneration System with Nanofluid-Based Parabolic Trough Collectors," *Energies*, vol. 10, no. 7, pp. 1-31, 2017. [CrossRef] [Google Scholar] [Publisher Link]

[17] Simin Anvari, Rahim Khoshbakhti Saray, and Keyvan Bahlouli, "Employing a New Optimization Strategy Based on Advanced Exergy Concept for Improvement of a Tri-Generation System," *Applied Thermal Engineering*, vol. 113, pp. 1452-1463, 2017. [CrossRef] [Google Scholar] [Publisher Link]

[18] Madhav Shridhar Phadke, *Quality Engineering Using Robust Design*, Prentice-Hall, pp. 1-250, 1995. [Google Scholar] [Publisher Link]